Three-Dimensional Structure of ATP:Corrinoid Adenosyltransferase from *Salmonella typhimurium* in Its Free State, Complexed with MgATP, or Complexed with Hydroxycobalamin and MgATP[†,‡]

Cary B. Bauer,[§] Maris V. Fonseca,[ǁ] Hazel M. Holden,[§] James B. Thoden,[§] Thomas B. Thompson,[§] Jorge C. Escalante-Semerena,*[,ǁ] and Ivan Rayment*[,§]

Department of Biochemistry, University of Wisconsin, Madison, Wisconsin 53706, and Department of Bacteriology, University of Wisconsin, Madison, Wisconsin 53706

ABSTRACT: In *Salmonella typhimurium*, formation of the cobalt−carbon bond in the biosynthetic pathway for adenosylcobalamin is catalyzed by the product of the *cobA* gene which encodes a protein of 196 amino acid residues. This enzyme is an ATP:co(I)rrinoid adenosyltransferase which transfers an adenosyl moiety from MgATP to a broad range of co(I)rrinoid substrates that are believed to include cobinamide, its precursor cobyric acid and probably others as yet unidentified, and hydroxocobalamin. Three X-ray structures of CobA are reported here: its substrate-free form, a complex of CobA with MgATP, and a ternary complex of CobA with MgATP and hydroxycobalamin to 2.1, 1.8, and 2.1 Å resolution, respectively. These structures show that the enzyme is a homodimer. In the apo structure, the polypeptide chain extends from Arg[28] to Lys[181] and consists of an α/β structure built from a six-stranded parallel β-sheet with strand order 324516. The topology of this fold is very similar to that seen in RecA protein, helicase domain, F_1ATPase, and adenosylcobinamide kinase/adenosylcobinamide guanylyltransferase where a P-loop is located at the end of the first strand. Strikingly, the nucleotide in the MgATP·CobA complex binds to the P-loop of CobA in the opposite orientation compared to all the other nucleotide hydrolases. That is, the γ-phosphate binds at the location normally occupied by the α-phosphate. The unusual orientation of the nucleotide arises because this enzyme transfers an adenosyl group rather than the γ-phosphate. In the ternary complex, the binding site for hydroxycobalamin is located in a shallow bowl-shaped depression at the C-terminal end of the β-sheet of one subunit; however, the active site is capped by the N-terminal helix from the symmetry-related subunit that now extends from Gln[7] to Ala[24]. The lower ligand of cobalamin is well-ordered and interacts mostly with the N-terminal helix of the symmetry-related subunit. Interestingly, there are few interactions between the protein and the polar side chains of the corrin ring which accounts for the broad specificity of this enzyme. The corrin ring is oriented such that the cobalt atom is located ~6.1 Å from C5′ of the ribose and is beyond the range of nucleophilic attack. This suggests that a conformational change occurs in the ternary complex when Co(III) is reduced to Co(I).

Cobalamin is the largest cofactor utilized in biological systems and consists of a highly decorated corrin ring at the center of which lies a cobalt atom (Figure 1). The cobalt atom is hexacoordinate where four of the positions are filled by nitrogen atoms belonging to the tetrapyrrole and the other two positions are occupied by the upper and lower ligands.

The lower ligand is usually a 5,6-dimethylbenzimidazole moiety that is covalently attached to the corrin ring via a nucleotide loop. The upper ligand is variable; however, the biologically functional forms of cobalamin have either an adenosyl or methyl group covalently attached to the cobalt. The unusual chemistry associated with cobalamin-dependent enzymes is the result of a labile single cobalt−carbon bond between the cobalt atom and the upper ligand.

The carbon−metal bond is unique in biological systems, and as a consequence, considerable effort has been devoted toward understanding the cobalamin biosynthetic pathway and the enzymes that utilize this cofactor. The identity of the chemical steps and the enzymes involved in the aerobic pathway were first elucidated for *Pseudomonas denitrificans* (*1*). Likewise, there is considerable knowledge of the anaerobic pathway in *Salmonella typhimurium* (*2*). To date, 25 gene products have been identified for the synthesis of adenosylcobalamin; however, the identity of the enzymes involved in the synthesis of the lower ligand base 5,6-dimethylbenzimidazole remains unknown. There is still
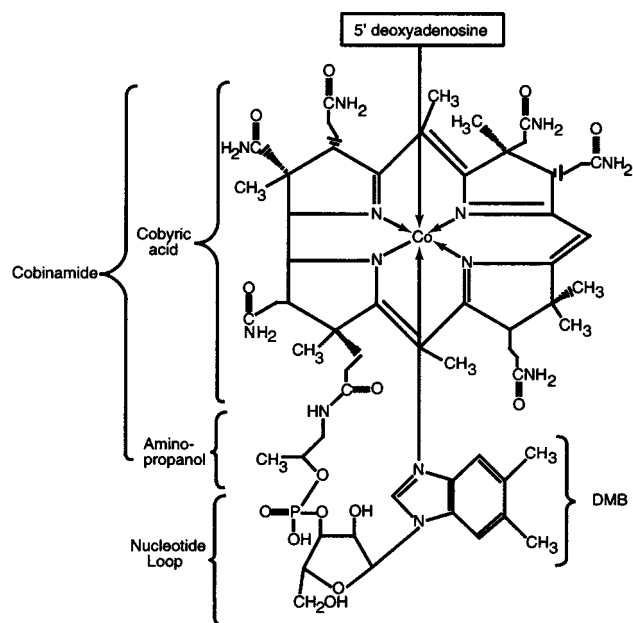
FIGURE 1: Chemical structure of 5′-deoxyadenosylcobalamin. In *S. typhimurium*, the lower ligand is 5,6-dimethylbenzimidazole (*45*).

considerably more to be learned about the organization, structure, and function of the proteins that are responsible for this remarkable feat, especially since there appear to be significant differences between the aerobic and anaerobic biosynthetic pathways. One of the variables appears to be the timing of cobalt insertion and the formation of the cobalt−carbon bond (*3, 4*). This is especially intriguing because it involves the formation of the molecular feature that is ultimately responsible for the final function of cobalamin.

In *P. denitrificans*, cobalt is inserted into the corrinoid in the biosynthetic pathway after synthesis of hydrogenobyrinic acid a,c-diamide by the enzyme cobaltochelatase (*5*). Thereafter, adenosylation occurs to yield adenosylcobyrinic acid a,c-diamide (*6*). In contrast, insertion of cobalt and adenosylation is thought to occur much earlier in the anaerobic biosynthetic pathway of *S. typhimurium*, perhaps as early as cobalt-precorrin 3 (M. V. Fonseca and J. C. Escalante-Semerena, unpublished results). This suggests that the substrate specificity of the intervening biosynthetic enzymes in the aerobic and anaerobic pathways must be different to accommodate the absence or presence of the adenosyl group.

In both *P. denitrificans* and *S. typhimurium*, adenosylation of the central cobalt atom occurs in a three-step process: (1) the cobalt is reduced from Co(III) to Co(II) in a one-electron transfer, (2) Co(II) is reduced to Co(I) in a second single-electron transfer to generate a very powerful nucleophile, and finally, (3) the Co(I) conducts a nucleophilic attack on the adenosyl moiety of ATP to leave the cobalt atom in a Co(III) state. Several corrinoid reductase activities have been reported, some of which have been isolated from a variety of organisms (*7−11*); however, the identity of the genes encoding these enzymes is still unknown. There is good evidence that flavin nucleotides are involved in the reduction of the cobalt since cell-free extracts from both *Clostridium tetanomorphum* and *Proprionibacterium freundenreichii* require these cofactors for function (*11, 12*). Likewise, in *Escherichia coli*, a flavodoxin has been shown

to catalyze the reduction of cobalamin when bound to methionine synthase (*13, 14*); however, a recent study of the adenosylation reaction in *S. typhimurium* has demonstrated that reduction from Co(III) to Co(II) can be accomplished by the dihydroflavins alone without an enzymatic partner (*15*). Regardless of the manner in which the cobalt atom is reduced, it seems highly likely that the final reduction from Co(II) to Co(I) must occur on the enzyme responsible for the adenosyl transfer because of the reactivity of Co(I).

The enzyme responsible for the adenosylation reaction is the product of gene *cobO* in *P. denitrificans* and *cobA* in *S. typhimurium* (*6, 16*). Both of these enzymes have been purified and partially characterized (*6, 17*). In the case of CobO from *P. denitrificans*, the enzyme shows specificity for cobyrinic acid a,c-diamide and the corrinoids that occur later in the biosynthetic pathway. Studies on CobA from *S. typhimurium* suggest broader specificity for this enzyme since the cobalt ion is inserted earlier than in *P. denitrificans*; however, the exact point of adenosylation is unknown. Broad specificity for CobA might be of some evolutionary advantage since it allows corrinoids that have lost their upper ligand to be recycled and it facilitates entry of exogenous corrinoids into the biosynthetic pathway. Interestingly, CobA is able to transfer a variety of nucleosides to the cobalt, including CTP, UTP, and GTP in decreasing order of preference (*17*).

Nucleophilic attack of Co(I) on the ribosyl moiety of the nucleotide is believed to heterolytically displace triphosphate. Earlier studies on the transferase activity in *C. tetanomorphum* demonstrated that the product is triphosphate (*18*), while in *Pr. freundenreichii*, the orthophosphate and pyrophosphate were reported to be the product of the reaction catalyzed by the adenosyltransferase enzyme (*12*); however, neither protein was characterized in detail. In the case of the enzyme from *P. denitrificans*, the exact nature of the product is still unknown, while for CobA from *S. typhimurium*, unpublished findings indicate that the product is likewise triphosphate (M. V. Fonseca and J. C. Escalante-Semerena, unpublished results).

The reaction catalyzed by this enzyme poses several interesting questions with respect to the substrate specificity and the oxidation state of the substrate. First, how does the protein coordinate the reduction of Co(II) to Co(I) and the transferase activity? Second, what is the relationship between the nucleotide and the cobalt prior to nucleophilic attack since there is good evidence that the nucleotide must bind before the corrinoid (*17*)? Third, what features of the enzyme allow it to accommodate corrinoids that differ widely in the substitution of their corrin rings? To address these questions, a structural and biochemical investigation of CobA from *S. typhimurium* was initiated. Here we report the X-ray structures of ATP:corrinoid adenosyltransferase from *S. typhimurium* (CobA) in its substrate-free state (apo), complexed with MgATP, and in a ternary complex with CobA, hydroxycobalamin, and MgATP determined to 2.1, 1.8, and 2.1 Å resolution, respectively.

MATERIALS AND METHODS

Purification and Overproduction of the ATP:Corrinoid Adenosyltransferase (CobA). Overproduction and purification of the CobA enzyme were performed as previously described with some modifications (*17*), including monitoring via

SDS−PAGE[1] (*19*) and employing the in vitro corrinoid adenosylation assay.

Cells of strain JE2884 [*metE205 ara-9* DEL902(*cobA-trp*)/ pGP1-2, pCOBA15] were grown in 6 L of Luria-Bertani (LB) broth containing ampicillin (50 μg/mL), kanamycin (50 μg/mL), and 22 mM glucose at 30 °C with shaking until they reached an A_{650} of ∼0.7. Cultures were shifted to 42 °C for 30 min and then to 37 °C for 1.5 h to allow synthesis of CobA. The resultant cells were pelleted by centrifugation in a Sorvall centrifuge (DuPont Instruments, Wilmington, DE) at 10000g utilizing a Sorvall GSA rotor.

These cells were resuspended in 150 mL of 50 mM Tris-HCl buffer (pH 8.0) at 4 °C which contained 5 mM DTT (buffer A) and 16 μg/mL protease inhibitor and phenyl-methanesulfonyl fluoride. The cell suspension was lysed by sonication with a Sonic Dismembrator (model 550 Fisher Scientific) for 7.5 min (large tip, setting of 6, 50% duty). Cell-free extracts were obtained by centrifugation at 40000g for 2 h on a Sorvall TYPE-SS34 rotor (Sorvall Instruments, Newtown, CT). Approximately 6.5 mg of protein was obtained per milliliter of cell-free extract.

Precipitation of proteins in the cell-free extract was performed at 4 °C using finely ground Ultrapure ammonium sulfate (ICN Biochemicals, Aurora, OH). Ammonium sulfate was added to the cell-free extract to 25% saturation. The protein solution was centrifuged at 10000g for 10 min to remove precipitated material from the first step. Following centrifugation, ammonium sulfate was added to 45% saturation. The precipitated protein was collected by centrifugation as described above.

Hydrophobic Interaction Chromatography. The protein pellet from the previous step was resuspended in 70 mL of buffer A containing 20% saturation ammonium sulfate. The protein solution was loaded onto a Phenyl-Sepharose (Sigma Chemical Co., St. Louis, MO) column (2.5 cm × 14 cm, 70 mL bed volume) equilibrated with buffer A containing 20% ammonium sulfate. The column was developed at a flow rate of 54 mL/h. Protein was loaded at a concentration of 10 mg/mL of resin. The column was washed with 250 mL of the loading buffer followed by a 350 mL reverse linear gradient (from 20 to 0%) of ammonium sulfate in buffer A. CobA eluted at the end of the gradient.

Dye−Ligand Affinity Chromatography. Fractions from the Phenyl-Sepharose step containing CobA were pooled. Potassium chloride (KCl) was added to the pool of fractions to a final concentration of 0.2 M. A Cibacron Blue 3GA Type 3000 (Sigma) column (1.5 cm × 11 cm, 20 mL bed volume) was equilibrated with buffer A containing 0.2 M KCl and developed at a flow rate of 60 mL/h. Approximately 6.8 mg of protein/mL of resin was loaded. After the column had been washed with 60 mL of equilibration buffer, a 100 mL linear gradient of from 0.2 to 2 M KCl was used to develop the column. CobA was ∼95% homogeneous as judged by SDS−PAGE. Fractions containing homogeneous CobA were pooled and concentrated with a Centriprep 10 device (Amicon, Inc., Beverly, MA). This protocol yielded between

30 and 50 mg of homogeneous CobA from 6 L of cells, depending on the level of overexpression.

Purification and Overproduction of Selenomethionine−CobA (SeMet−CobA). SeMet−CobA was also overproduced from strain JE2884. Cells of strain JE2884 were grown on Vogel-Bonner minimal medium (*20*) supplemented with glucose (35 mM). All amino acids, except methionine, were added to a final concentration of 5 mM. Additionally, the medium was supplemented with 5 mM adenine and SeMet (5 mM). SeMet−CobA was purified according to the protocol described for the wild-type enzyme (see above). All buffers used in the SeMet−CobA purification were sparged with oxygen-free nitrogen 30−45 min before use. Fractions containing purified SeMet−CobA were pooled and kept at 4 °C under a nitrogen atmosphere in the presence of 5 mM DTT. Approximately 30 mg of homogeneous SeMet−CobA was obtained from this procedure.

Apo-CobA Crystallization X-ray Data Collection and Structure Determination. Crystals of CobA (both wild type and SeMet) were grown by microbatch at 4 °C from 13% methyl ether-polyethylene glycol 350 and 100 mM NaCl in 50 mM MES (pH 5.5). The final protein concentration in each droplet was approximately 5 mg/mL. Small hexagonal plate-shaped crystals appeared spontaneously in 3−4 days and achieved maximum dimensions 0.1 mm × 0.4 mm × 0.4 mm over a period of several weeks.

Prior to X-ray data collection, crystals of the seleno-methionine-substituted apo-CobA were transferred to a synthetic mother liquor composed of 25% methyl ether-polyethylene glycol 350 and 250 mM NaCl in 50 mM MES (pH 5.5) and allowed to equilibrate at 4 °C overnight. Crystals were then transferred incrementally to a cryoprotectant solution consisting of 25% ethylene glycol, 20% methyl ether-polyethylene glycol 350, and 300 mM NaCl, in 50 mM MES (pH 5.5). The crystals were transferred successively to droplets with 30, 50, and 100% cryoprotectant/synthetic mother liquor ratios and allowed to stand for 1 min. A single crystal was picked up in a loop of surgical suture and flash-frozen in a stream of cold liquid nitrogen gas. Apo-CobA crystallizes in the hexagonal space group $P6_122$ with one subunit in the asymmetric unit and the following unit cell dimensions: $a = b = 49.4$ Å and $c = 250.2$ Å.

Multiple anomalous dispersion (MAD) data were collected at four wavelengths on a single frozen crystal at beamline 19-ID of the Structural Biology Center at the Advanced Photon Source in Argonne, IL. For each wavelength, 100 images were recorded on a 3 × 3 tiled CCD detector with 1° oscillations. An additional 100, 1° images were then recorded with a ϕ value that differed by 180° from the original images (inverse beam method). The diffraction data were processed and scaled with the HKL2000 software suite (*21*). The Friedel differences in the reference data set (peak) were externally locally scaled to remove systematic errors with the program BIGSCALE (G. Wesenberg and I. Rayment, unpublished data). The other three data sets were then locally scaled to the reference data set. Data collection and processing statistics are presented in Table 1.

The positions of five of the seven selenium atoms were located with automated Patterson methods utilized by the program SOLVE (*22*, *23*). Phases were then calculated from the MAD data sets with the program CNS (*24*). Density

Table 1: X-ray Data Collection Statistics

| | apo-CobA | | | | | MgATP·CobA | OH-CBL·CobA | | | |
| | SeMet | | | | | | SeMet | | | wild-type |
	remote 1	peak	edge	remote 2	native[a]	wild-type	peak	edge	remote	native
wavelength (Å)	0.94290	0.97939	0.97960	1.0205	0.97939	0.7009	0.97923	0.97947	0.98325	0.908
X-ray source	APS 19-ID	APS 19-ID	APS 19-ID	APS 19-ID	APS 19-ID	APS 19-ID	APS 19-ID	APS 19-ID	APS 19-ID	SSRL 7-1
resolution (Å)	2.6	2.6	2.6	2.6	2.19 (2.18–2.10)	1.8 (1.86–1.8)	2.5	2.5	2.5	2.05 (2.12–2.05)
no. of unique reflections	6977	6998	6968	6255	10494 (698)	17014 (1357)	18240	18212	18157	29124 (2803)
redundancy	3.4	3.3	3.3	3.3	6.0 (2.5)	8.3 (4.7)	5.8	5.8	5.6	4.6 (3.9)
completeness (%)	98.3 (98.4)	98.2 (97.8)	98.3 (98.4)	98.2 (98.3)	90.7 (63.2)	93.3 (63.2)	98.2 (98.4)	98.3 (99.4)	97.3 (98.2)	98.1 (97.1)
avgerage I/σ	35.6	52.5	51.9	64.7	35.9 (7.2)	31.6 (3.0)	28.5	26.7	25.7	24.3 (3.6)
R-merge[b]	0.054	0.057	0.041	0.033	8.2 (17.7)	6.1 (31.1)	0.085	0.096	0.073	5.5 (28.1)

[a] Numbers in parentheses represent the statistics for the highest-resolution shell. [b] R-merge $= (\sum|Ihkl\text{-}I|/(\sum Ihkl)$ where the average intensity I is taken over all symmetry equivalent measurements and Ihkl is the measured intensity for a given reflection.

Table 2: Refinement Statistics[a]

	apo-CobA	apo-Coba·MgATP	OH-CBL·CobA
resolution limits (Å)	30.0–2.1	30–1.8	30–2.1
R-factor[b]	17.8	19.2	20.6
R-free	24.7	26.7	28.8
no. of reflections (working set)	10482	14575	29095
no. of reflections (test set)	1033	1435	2943
no. of protein atoms	1216	1212	2774
no. of solvent atoms	137	164	447
no. solvent molecules	136 H$_2$O, 1 Cl$^-$	132 H$_2$O, 1 ATP, 1 Mg^{2+}	1 OH-CBL, 2 Mg^{2+}, 2 ATP, 292 H$_2$O
multiple conformations	Asn[97], Glu[141]	Gln[110], MgATP	Glu[141]
average B value for main chain atoms	20.0	26.3	35.3
average B value for all protein atoms	24.2	30.6	39.1
average B value for solvent atoms	45.4	50.1	46.0
weighted rms deviations from ideality			
bond lengths (Å)	0.017	0.015	0.015
bond angles (deg)	2.58	2.73	2.60
planarity (trigonal) (Å)	0.007	0.003	0.008
planarity (others) (Å)	0.009	0.007	0.013
torsional angles (deg)	16.6	16.8	17.7

[a] TNT refinement. [b] R-factor $= \sum||F_o| - k|F_c||/\sum|F_o| \times 100$.

modification (solvent flipping) was performed with CNS (24). This procedure yielded an electron density map that showed continuous electron density over a large region of the unit cell. Residues Arg[28]–Lys[181] were built into the electron density with the program TURBO FRODO (25) and refined with TNT (26). The missing residues at the N- and C-termini could not be located in the electron density map. Analysis of the backbone dihedral angles with PROCHECK revealed that for the apo-CobA, 95.5% of the residues conformed to the most favorable regions and the other 4.5% conformed to other additionally allowed regions (27). The final R-factor was 17.8% for X-ray data between 30 and 2.1 Å resolution with an R-free of 24.7%. The final refinement statistics are presented in Table 2.

MgATP·CobA Structure Determination. Crystals of apo-CobA described above were transferred to a solution that contained 25% methyl ether-polyethylene glycol 350, 250 mM NaCl in 50 mM MES, 1 mM MgATP, and 1 mM OH-CBL at pH 5.5. The crystals were then frozen as before except for the inclusion of MgATP and OH-CBL in the solutions. The X-ray data were recorded at a single wavelength at beamline 19-ID of the Structural Biology Center at the Advanced Photon Source in Argonne, IL. One hundred eighty images were recorded on a 3 × 3 tiled CCD detector with 1° oscillations. The diffraction data were processed and scaled with the HKL2000 software suite (21). The structure was determined by molecular replacement starting from the apo structure and refined with TNT (26). Electron density was clearly visible for residues Glu[27]–Ala[183] together with the MgATP ligand. Although the density for the triphosphate moiety is well-defined, the adenine group appears to adopt multiple conformations within the nucleotide binding site. There was no evidence for hydroxycobalamin even though it was included in the transfer solutions. Analysis of the backbone dihedral angles with PROCHECK revealed that for the MgATP·CobA complex, 94.7% of the residues conformed to the most favorable regions, whereas the other 5.3% conformed to other additionally allowed regions (27). The final R-factor was 19.2% for X-ray data between 30.0 and 1.8 Å resolution with an R-free of 26.7%. The final refinement statistics are presented in Table 2.

Hydroxycobalamin–CobA Crystallization. Prior to crystallization, dilute CobA (2 mg/mL) was mixed with 2 mM ATP, 2 mM MgCl$_2$, and 2 mM hydroxycobalamin (OH-CBL). The protein solution was allowed to stand on ice for 30 min and then concentrated to 10 mg/mL. Crystals of the OH-CBL· CobA complex were grown from microbatch at 4 °C from a range of 5–9% polyethylene glycol 3350 with 300 mM NaCl in imidazole buffer at pH 7.0. Small rod-shaped crystals appeared overnight. A large number of crystals appeared in each well and stopped growing after a period of 2–3 days regardless of the polyethylene glycol concentration present. To combat this problem, each well was fed with 4 μL of a fresh polyethylene glycol/CobA solution (at the original

polyethylene glycol concentration) every other day for a period of 2 weeks. With this method, crystals achieved maximum dimensions of 0.1 mm × 0.1 mm × 0.5 mm.

Hydroxycobalamin−CobA Data Collection and Structure Determination. Prior to X-ray data collection, crystals of the OH-CBL·CobA complex were transferred to a synthetic mother liquor containing 18% polyethylene glycol 3350, 300 mM NaCl, and 0.5 mM OH-CBL in 50 mM imidazole (pH 7.0) and allowed to equilibrate overnight at 4 °C. A cryoprotectant solution containing 18% polyethylene glycol 3350, 20% ethylene glycol, 300 mM NaCl, and 1 mM OH-CBL in 50 mM imidazole at pH 7.0 was prepared. The crystals were first transferred into a 1:1 mixture of synthetic mother liquor and cryoprotectant and allowed to stand for 5 min. Subsequently, they were transferred to a droplet of straight cryoprotectant solution. A single crystal was picked up in a loop of surgical suture and flash-frozen in a stream of cold liquid nitrogen gas. Crystals of CobA were shown to belong to either the space group $P4_{3}2_{1}2$ or $P4_{1}2_{1}2$ by precession photography with two subunits per asymmetric unit and the following unit cell dimensions: $a = b = 79.4$ Å and $c = 141.7$ Å.

Multiple anomalous dispersion (MAD) data were collected at four wavelengths on a single frozen crystal at beamline 19-ID of the Structural Biology Center at the Advanced Photon Source in Argonne, IL. For each wavelength, 180 images were recorded on a 3 × 3 tiled CCD detector with 1° oscillations. The diffraction data were processed and scaled using the HKL2000 software suite (*21*). The Friedel differences in the reference data set (peak) were externally locally scaled to remove systematic errors with the program BIGSCALE (I. Rayment and G. Wesenberg, unpublished results). The other three data sets were then locally scaled to the reference data set. X-ray data collection and processing statistics are presented in Table 1.

The positions of the selenium atoms could not be readily located by any programs utilizing automated Patterson methods (SOLVE or CNS), by direct methods (SHELXS-97 or Shake-n-Bake), or by manual examination of anomalous Patterson maps. It was eventually deduced that a 2-fold noncrystallographic axis was positioned in the unit cell such that it lay parallel to a crystallographic 4-fold axis. The result of this noncrystallographic symmetry was that many of the Patterson vectors overlap on the Harker section, resulting in one large peak. This interpretation was later shown to be correct once the positions of the selenium atoms were known.

The positions of five of seven selenium atoms were ultimately located by molecular replacement utilizing the apo structure as a phasing model. These positions were deduced from appropriate anomalous dispersion difference maps and refined with the program CNS (*24*). The phases were improved by extensive cyclic solvent flattening and 2-fold averaging with the program DM (*28, 29*), which yielded an electron density map that showed continuous electron density for a CobA dimer, as well as unambiguous density for hydroxycobalamin and MgATP molecules in one-half of the dimer. The temperature factors for the hydroxycobalamin are very similar to those of the protein, which suggests full occupancy for this ligand. No cobalamin density was observed in the opposite half of the dimer. Residues Arg[28]−Tyr[196] for monomer A and residues Gln[7]−Tyr[196] for monomer B were built into the electron density with TURBO

FRODO (*25*). At this point, the refinement was continued against a higher-resolution data set recorded at the Stanford Synchrotron Radiation Laboratory. At this stage, MgATP was built into both subunits together with one molecule of hydroxycobalamin. The structure was refined with TNT (*24, 26*). Analysis of the backbone dihedral angles with PROCHECK revealed that for the OH-CBL·CobA complex, 90.1% of the residues conformed to the most favorable regions and the other 9.1% conformed to other additionally allowed regions (*27*). The final *R*-factor was 20.6% for X-ray data between 30.0 and 2.1 Å resolution with an *R*-free of 28.8%. Refinement statistics are presented in Table 2. The X-ray coordinates and structure factos have been deposited in the Protein Data Bank under file names 1G5R, 1G5T, and 1G64 for the apo-CobA, MgATP·CobA, and OH-CBL·CobA complex, respectively.

RESULTS AND DISCUSSION

Structure of Apo-CobA. The final model of apo-CobA contains 154 amino acid residues out of 196 expected from the amino acid sequence together with 136 water molecules. The polypeptide chain extends without breaks from Arg[28] to Lys[181]. A representative section of the electron density is shown in Figure 2a. In the apo structure, the N- and C-terminal regions of the polypeptide chain are disordered; however, as noted later, these are well-defined in the presence of both MgATP and hydroxycobalamin. A ribbon representation of apo-CobA is displayed in Figure 3a. The core domain of the protein, which extends from Arg[28] to Ala[183], consists of an α/β structure that is centered on a six-stranded parallel β-sheet with strand order 324516. The strands are connected by five α-helices that lie on both sides of the sheet as expected from the strand order. The topology of this fold is very similar to that seen in RecA protein, F_{1}ATPase, helicase core domain, and adenosylcobinamide kinase/adenosylcobinamide guanylyltransferase (*30−33*), all of which belong to the P-loop-containing family of nucleotide hydrolases as shown in Figure 4. Consistent with this classification, CobA contains a P-loop motif (GNGKGKT) defined by residues Gly[36]−Thr[42] (*16, 34*). In this case, however, the motif contains only seven residues rather than the eight or nine typically observed in other members of the family (*35, 36*). In CobA, the P-loop resides at the end of the N-terminal strand in the sequence and is flanked by only one other strand at the edge of the sheet (strand 6 in the sequence). As shown later, the manner in which ATP is coordinated by the P-loop is unique to CobA, differing from all other members of the nucleotide hydrolase superfamily. Even so, the topological similarity of CobA to other members of this group suggests that this enzyme evolved from a primordial kinase or nucleotide hydrolase.

The arrangement of secondary structural elements in CobA serves to generate a large bowl-shaped cavity that lies at the C-terminal ends of the β-strands. This depression is formed by the loops that connect the β-strands and their succeeding α-helices. The P-loop lies on one side of this large cavity and serves to identify the location of the active site.

Tertiary Structure. CobA is a homodimer, where the two subunits are related by a crystallographic 2-fold in the apo structure (Figure 3b). The total surface area buried by dimer formation is ~2870 Å^2 as determined with the program
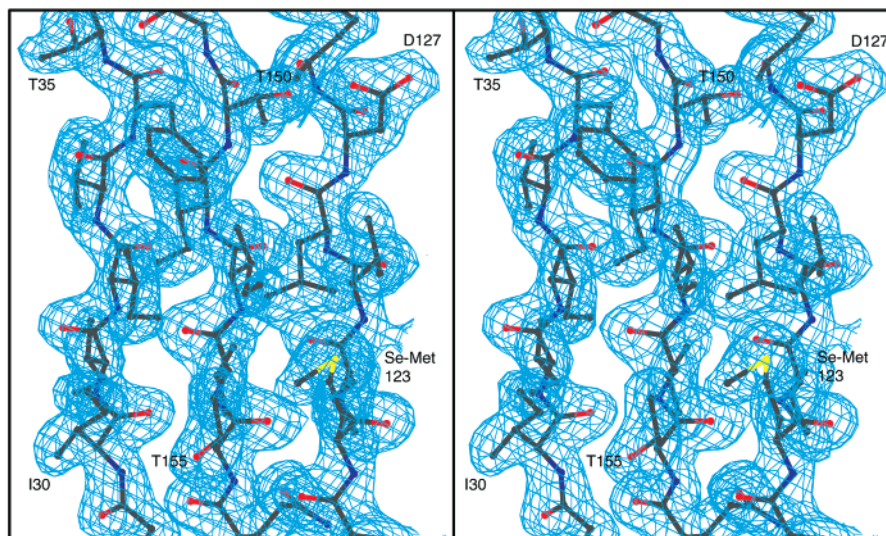
FIGURE 2: Stereoview of representative electron density corresponding to the apo-CobA structure. The map was calculated with coefficients of the form $2F_o - F_c$. This figure was prepared with the programs Molscript and Bobscript (*46*, *47*).

AREAIMOL in the CCP4 program package (*28*). This substantial subunit interface is dominated by an antiparallel interaction formed between the last strand ($\beta6$) of the sheet of one subunit (including its C-terminal extension) and the symmetry-related motif (Figure 3b). It is noteworthy that the C-terminal extensions make extensive contacts at the subunit—subunit interface. The symmetry-related interactions between the α-helices that follow the P-loop also contribute substantially to the buried surface area.

Structure of the MgATP·CobA Complex. The location of the MgATP binding site in CobA was identified by soaking the apo crystals in MgATP. Except for the region of polypeptide chain immediately surrounding the nucleotide substrate, the structural changes were quite small. The rms difference between the apo structure and the MgATP complex was 0.16 Å for 149 structurally equivalent α-carbons as determined with the program ALIGN (*37*). As shown in Figure 5a, the electron density corresponding to the three phosphates of the nucleotide is unambiguous. In contrast, however, the ribose and adenine moieties appear to adopt multiple conformations (A and B) and are less well defined in this complex. As expected, the phosphates are coordinated by the P-loop, but remarkably, the orientation of the triphosphate moiety is opposite to that observed in all other nucleotide-dependent enzymes that utilize this motif. There are comparatively few interactions between the protein and the adenosine moiety for either conformation in this complex (Figure 5a). Orientation A for the ATP is the same as that observed in the hydroxycobalamin—CobA complex described later, whereas conformation B appears to reflect the greater structural freedom of the nucleotide in the absence of the corrinoid. A detailed description of the protein—MgATP interactions is deferred until the discussion of the ternary complex. It is noteworthy, however, that the unusual conformation of MgATP is seen in the absence of the corrinoid.

Figure 5b shows the P-loop from the β-subunit of F_1ATPase (*31*) with bound AMP-PNP superimposed onto CobA with ATP in conformation A. As can be seen, the three phosphates and their associated magnesium ions lie nestled against the P-loop and occupy similar locations,

except that the α-phosphate of ATP in CobA lies in the same position as the γ-phosphate of AMP-PNP in F_1ATPase (and all other P-loop-containing enzymes). As a consequence, the adenosine of ATP in CobA extends across the end of the P-loop, whereas in F_1ATPase, the adenosine group lies against the α-helix that succeeds the P-loop. The comparison of CobA with F_1ATPase suggests why the P-loop in CobA is one residue shorter than the stereotypical motif. Removal of one amino acid residue flattens the loop and eliminates a steric clash that would otherwise occur.

It is highly unlikely that CobA could have evolved from a nucleotide hydrolase without changing the coordination of the nucleotide in a fundamental way for the following reason. In other hydrolases, the γ-phosphate is in a position to be transferred to either water or some another functional group (the aminopropanol group of adenosylcobinamide in CobU, for example). Typically, the γ-phosphate is somewhat exposed to a cavity that contains the attacking nucleophile. Conversely, in most enzymes that utilize a P-loop, the 5′-carbon of the ribose is buried in a nucleoside binding pocket. This simply could not work for the reaction catalyzed by CobA. In CobA, where the adenosyl group is transferred, inverse use of the P-loop leaves the 5′-carbon of the ribose exposed for nucleophilic attack. Clearly, this enzyme could not function as an adenosyltransferase if the nucleotide were bound in a conventional manner.

The conformation of ATP observed in CobA is also somewhat unusual. Rather than the extended conformation as seen in F_1ATPase, myosin, and the G-proteins (*31*, *36*), the nucleotide is folded back onto itself. The adenosine exhibits a C2′-endo conformation for the ribose in conjunction with an anti conformation for the adenine which are both common. In contrast, the torsional angle about the C4′−C5′ bond places the triphosphate moiety over the endo face of the sugar. The conformation of the sugar reflects the anticipated geometry for nucleophilic attack of the cobalt(I) of the corrinoid on the 5′-carbon of the sugar moiety as shown by the structure of the hydroxycobalamin·MgATP·CobA complex described below.

Structure of the OH-CBL·CobA Complex. The asymmetric unit of the ternary complex contains one dimer of CobA,
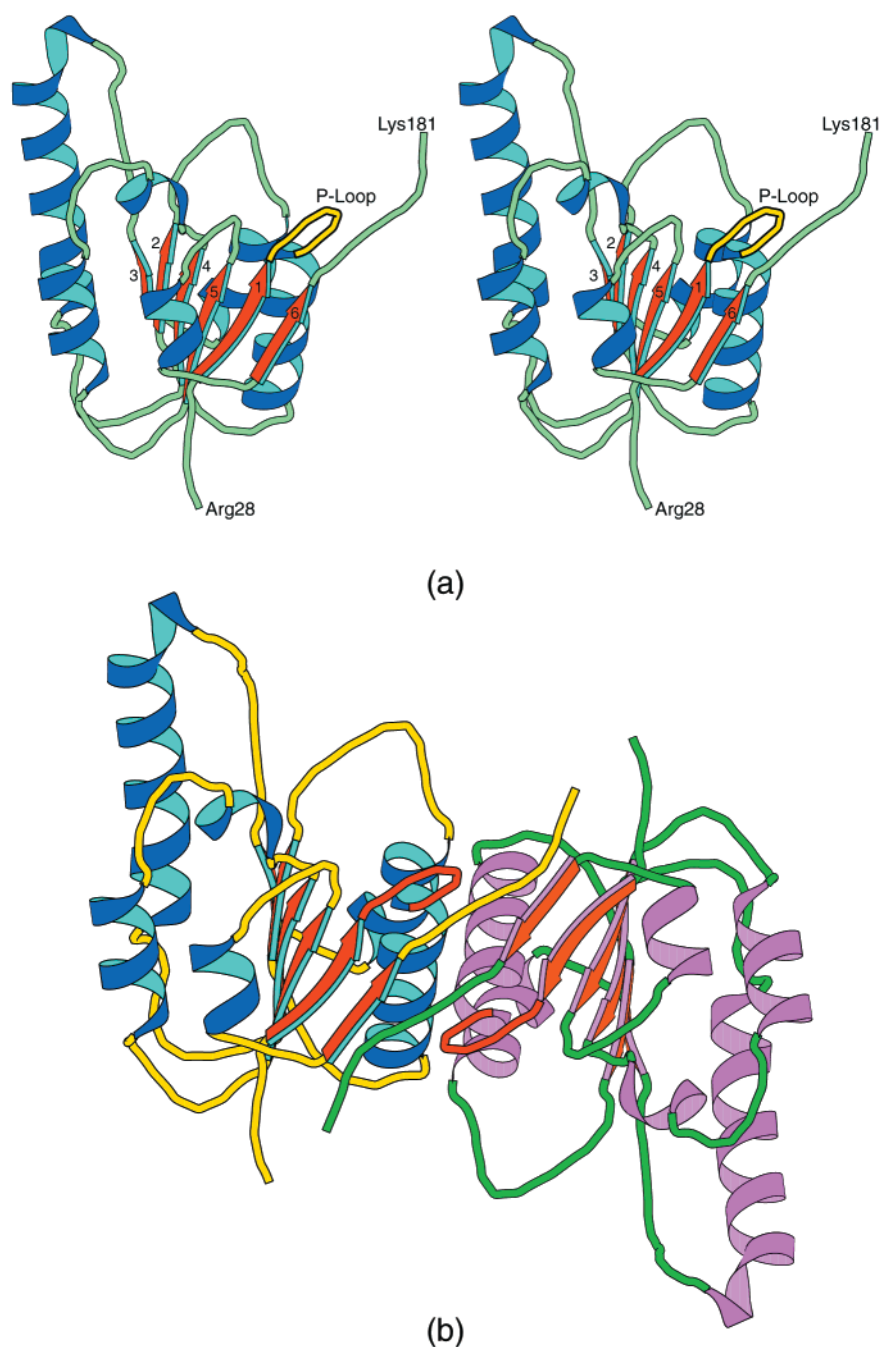
FIGURE 3: Ribbon representations of apo-CobA. A stereoview of one subunit of CobA where the P-loop is highlighted in yellow and the strands are numbered according to their order in the sequence is shown in panel a. A ribbon representation of the two crystallographically related subunits of CobA viewed approximately down the 2-fold axis of symmetry is displayed in panel b. The N- and C-terminal residues are disordered in the apo structure. The final amino acid residues of the C-terminus observed in the apo structure form a prominent interaction with those from the neighboring subunit. This figure was prepared with the programs Molscript and Bobscript (*46*, *47*).

two molecules of MgATP, and one molecule of hydroxycobalamin. The electron densities for the hydroxycobalamin and its associated MgATP are unambiguous and clearly define the orientations of the corrinoid, its nucleotide loop, and lower ligand as shown in Figure 6. The final model for the dimer of the OH-CBL·CobA complex contains 359 amino acid residues out of the 392 that are expected. The polypeptide chain extends without breaks from Arg[28] to Tyr[196] for subunit A and from Gln[7] to Tyr[196] for subunit B. A total of 447 solvent molecules were included in the model. Although there are two active sites per dimer, only one is occupied by hydroxycobalamin in the crystal. This is

probably an artifact of crystallization since the enzyme kinetics do not suggest anticooperativity (*17*). The active site that is missing the hydroxycobalamin does contain MgATP. This adopts a conformation similar to that seen in the active site that binds hydroxycobalamin and to that of conformation A of the MgATP·CobA complex. The following discussion will focus on the active site that displays the ternary complex.

As is evident from Figure 6, coordination of hydroxycobalamin is accompanied by the ordering of amino acid residues that were disordered in the apo and MgATP·CobA structures. The binding site for hydroxycobalamin is formed mostly from subunit A which forms a shallow bowl-shaped
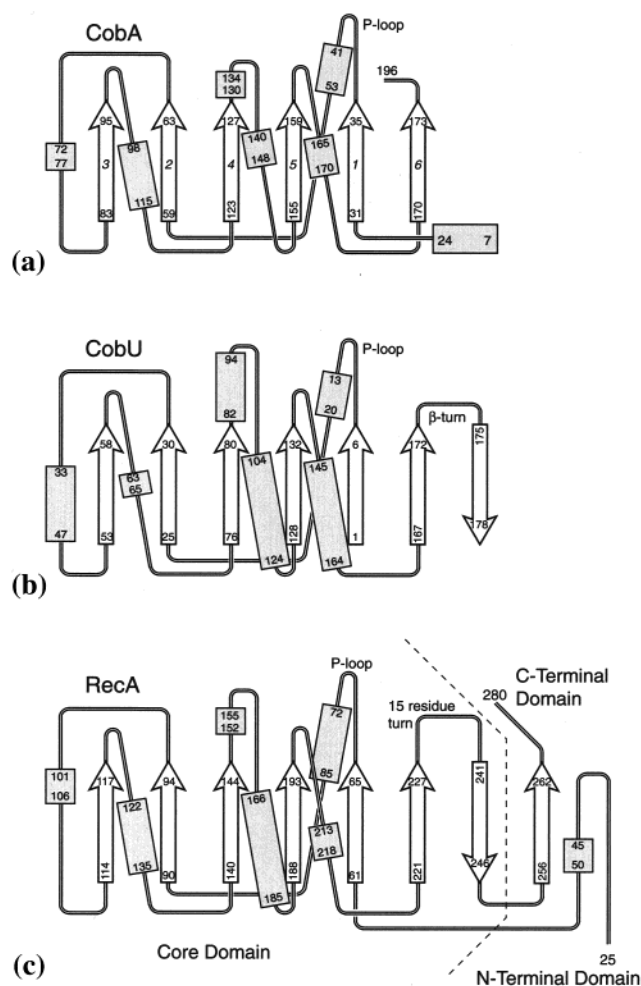
FIGURE 4: Topological drawings for (a) CobA (ATP:corrinoid adenosyl transferase), (b) CobU (adenosylcobinamide kinase/adenosylcobinamide phosphate guanylyltransferase), and (c) the RecA protein. The figure was prepared from coordinates from PDB entries 1G64, 1CBU, and 2REB (*30, 33*).

depression at the C-terminal end of the β-sheet; however, the active site is capped by the N-terminal helix from the symmetry-related subunit (B) that now extends from Gln[7] to Ala[24]. The corresponding amino acid residues in subunit A are disordered due to the absence of hydroxycobalamin in subunit B. As depicted in Figure 6, the corrin ring is located above the nucleotide where the cobalt atom is separated by a distance of ~6.1 Å from C5′ of the ribose.

MgATP Binding Site. A detailed view of the ternary complex is shown in Figure 7. As can be seen, the nucleotide is almost completely enclosed on one side by the protein and on the other side by the corrin ring. From the arrangement of MgATP and hydroxycobalamin, it is clear that the nucleotide must bind before the corrinoid as suggested from the kinetic behavior of CobA (*17*).

The electron density shows a well-defined magnesium ion that is octahedrally coordinated by two nonbridging phosphate oxygens from the α- and β-phosphates, the side chain hydroxyl of Thr[42], a carboxylate oxygen of Glu[128], and two water molecules. This coordination is very similar to that observed in subunit F of F_1ATPase, except for the carboxylate ligand. The latter ligand, if it exists in F_1ATPase, resides on a structurally different secondary structural element.

There are extensive contacts between the P-loop and the triphosphate moiety of ATP, as would be expected (Figures 7 and 8). All of the amino acid residues, except for Gly[36] and Gly[38], of the P-loop [defined by residues Gly[36]−Thr[42] (GNGKGKT)] are involved in coordinating the α-, β-, and γ-phosphates. Common to all proteins that utilize P-loops, there is extensive hydrogen bonding between the main chain amide hydrogens and the phosphoryl oxygens. As discussed above, the ATP is coordinated in the reverse manner to that observed in all other P-loop proteins. This has an interesting effect on the distribution of ligands since there is now an additional negative charge in the position normally occupied by the α-phosphate. The extra negative charge is neutralized by the inclusion of Arg[51′] (from the 2-fold related subunit) and Thr[43] in the coordination sphere of the γ-phosphate. The equivalent ligands are absent in other nucleotide binding proteins. Additional compensation for the negative charge on the α-phosphate is provided by positioning this group at the N-terminal end of the α-helix that follows the P-loop and allows the peptidic NH groups of Gly[40] and Thr[43] to contribute to the coordination sphere. It is noteworthy that there are very few differences in the positions of the side chains that coordinate MgATP between the apo structure and MgATP complex, except for Lys[39] which rotates away from the location that becomes occupied by the ribose.

In contrast to the triphosphate moiety of ATP, there are comparatively few hydrogen bonding interactions between the adenosine component and the protein. Only two hydrogen bonds are observed between Asp[195] and O3′ of the ribose and between the carbonyl oxygen of Asn[37] and the amino group of the adenine. This would account for the observed specificity of CobA toward nucleotide (*17*). Biochemical studies demonstrate that CobA exhibits 37% of the activity toward GTP relative to ATP, whereas the activities toward CTP and UTP were 98 and 88%, respectively. If GTP were to bind in a manner similar to that observed for ATP, it would introduce a carbonyl oxygen in proximity to Asp[195], which would be energetically unfavorable. Conversely, the pyrimidine rings of CTP or UTP might occupy the void left by the purine ring without introducing any unfavorable contacts and hence would not affect the kinetics under the conditions utilized for the assays.

Hydroxycobalamin Binding Site. Hydroxycobalamin binds on top of a bowl-shaped cavity at the C-terminal end of the β-strands that encloses MgATP (Figure 9). The corrin ring is roughly perpendicular to the plane of the β-sheet in such a way that the most of the amide groups that decorate the corrin ring are exposed to solvent, whereas the hydrophobic components are occluded by hydrophobic side chains. The corrinoid is abutted on two sides by loops that extend from β-strands 3, 4, and 6 and enclosed by the N-terminal α-helix from Gln[7′] to Gln[25′] of the adjacent subunit. Interestingly, the N-terminal α-helix interacts predominantly with the nucleotide loop of the hydroxycobalamin where it provides a salt bridge between Arg[16′] and a phosphate oxygen of the nucleotide loop together with a limited number of hydrophobic interactions from Thr[13′], Val[17′], and Val[21′]. This arrangement leaves the hydrophilic components of the corrin ring exposed to solvent.

The lower ligand of hydroxycobalamin, DMB, is clearly coordinated to the cobalt ion of the corrin ring where the Co−N bond distance is 2.2 Å. Ligand-on coordination was
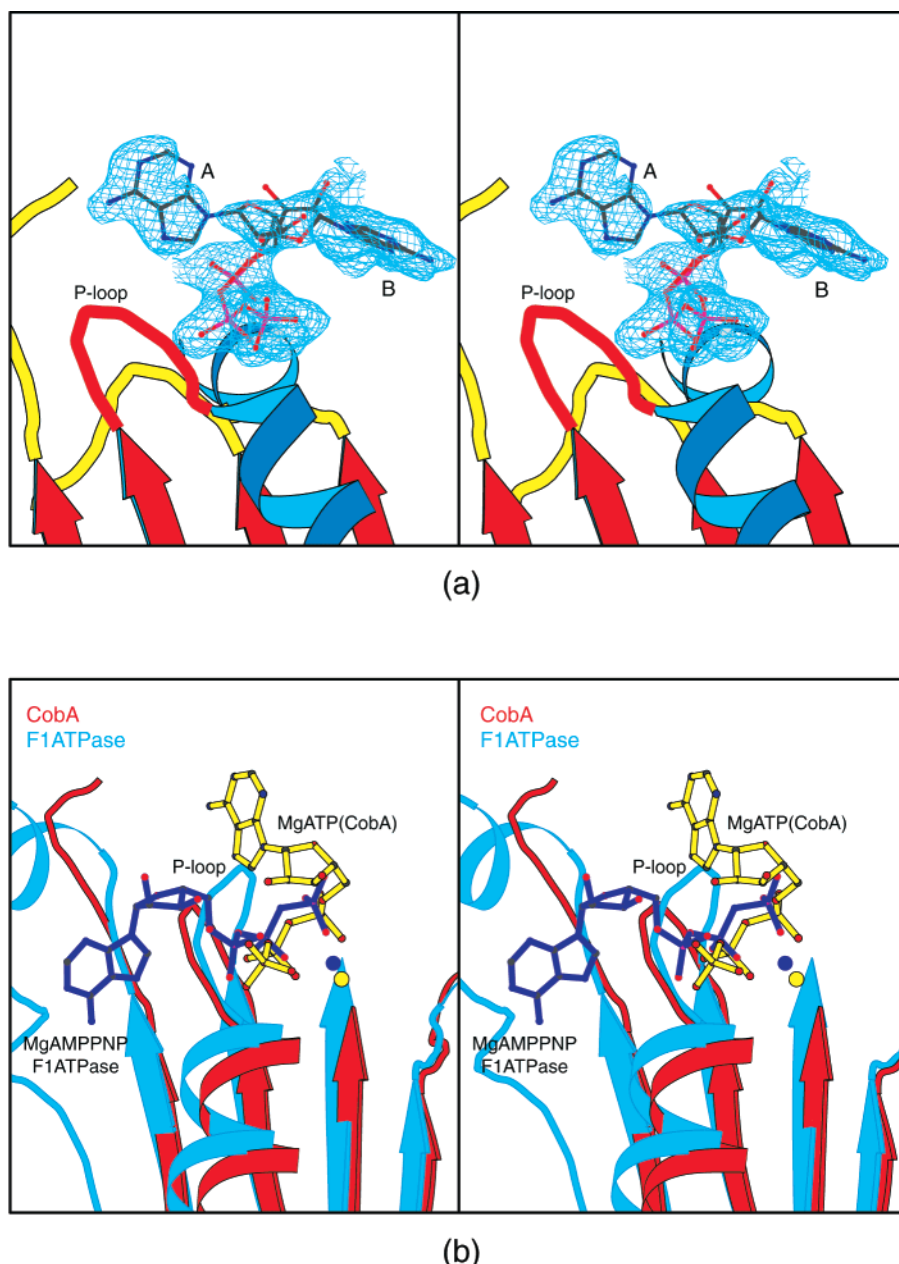
(a)

(b)

FIGURE 5: Electron density for MgATP and its orientation relative to the P-loop in F_1ATPase. Panel a shows a stereoview of the electron density for the two orientations of MgATP in CobA calculated with coefficients of the form $F_o - F_c$ where the substrate was omitted from the phase calculation. Panel b displays a part of the β-subunit of F_1ATPase together with its MgAMP-PNP superimposed onto the MgATP of CobA. F_1ATPase and MgAMP-PNP are depicted in cyan and blue, respectively, whereas CobA and MgATP are colored in red and yellow, respectively. The superposition was done with the program ALIGN (*37*) modified at the University of Wisconsin by G. Wesenberg to allow selection of the segments used for the alignment (available on request). The figure was prepared from coordinates from PDB entries 1COW (*31*) and 1G5T. This figure was prepared with the programs Molscript and Bobscript (*46*, *47*).

unexpected because of the ability of CobA to adenosylate both cob(I)inamide, which lacks the nucleotide loop, and cob-(I)alamin. It was also unexpected from the precedence established by the mode of binding of cobalamin observed in methionine synthase and methylmalonyl-CoA mutase since both of these show replacement of the lower ligand of cobalamin with a histidine side chain (*38*, *39*). Coordination of the cobalt by the lower ligand is utilized in some cobalamin-dependent enzymes, as observed in diol dehydratase (*40*). In CobA, it appears that the broad substrate specificity for the lower ligand is provided by conformational flexibility in the N-terminal α-helix.

Strikingly, there are very few hydrogen bonds between hydroxycobalamin and the protein. This absence of specific interactions between the hydrophilic components of the corrinoid is consistent with the anticipated broad specificity of this enzyme. As noted earlier, it is unknown for CobA at which point in the biosynthetic pathway the corrin ring becomes adenosylated; however, the orthologous enzyme from *P. denitrificans* is able to adenosylate cobyrinic acid and all of the subsequent intermediates in the biosynthetic pathway. It is expected that CobA from *S. typhimurium* will have even broader specificity since in this organism the cobalt is inserted considerably sooner. There are considerable differences between cobyrinic acid and hydroxycobalamin that potentially could have a profound influence on ligand binding, for example, amidation of six carboxylate groups. Thus, the corrin binding site must be able to accommodate
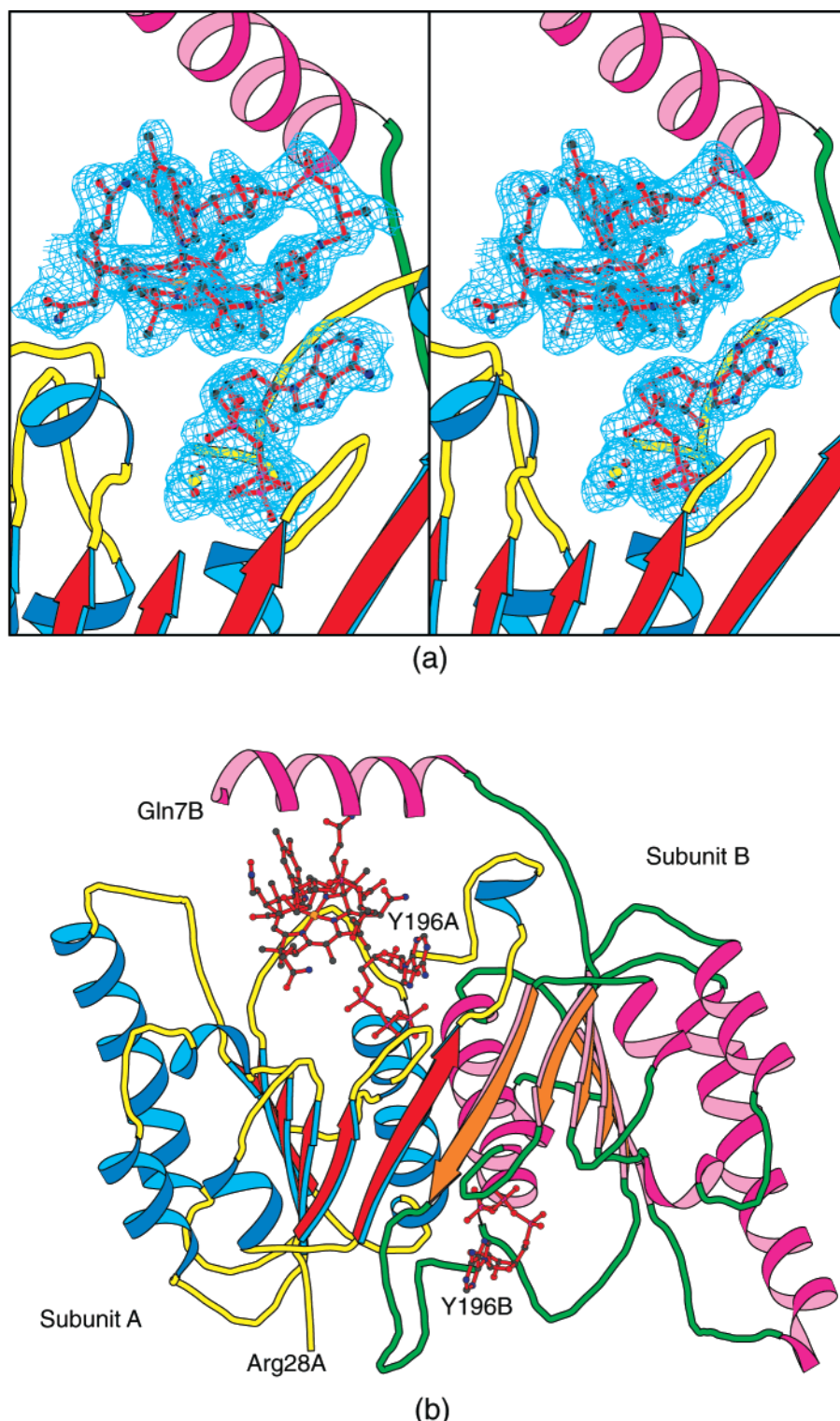
FIGURE 6: Ternary complex of CobA, MgATP, and hydroxycobalamin. A stereoview of the electron density for the hydroxycobalamin and MgATP is displayed in panel a. A ribbon representation of the OH-CBL·CobA complex viewed approximately down the noncrystallographic 2-fold axis is shown in panel b. The single hydroxycobalamin molecule observed in the lattice is coordinated mostly by subunit A. However, the N-terminus of subunit B is ordered in this complex and caps the active site where it interacts with the nucleotide arm and lower ligand. The electron density map was calculated with coefficients of the form $F_o - F_c$ where the ligands were omitted from the phase calculation. This figure was prepared with the programs Molscript and Bobscript (46, 47).

a wide range of substrates that differ greatly in ionic charge and state of assembly of the nucleotide loop. Exposure of the amide groups to solvent and the avoidance of any hydrogen bonding contacts would appear to be prerequisites for a binding site that can recognize such a diverse group of molecules. Likewise, the sparse interactions between the aminopropanol arm and nucleotide loop and the protein would also appear to be consistent with this structural theme. Again, the coordination of the corrinoid by CobA differs considerably from that seen in cobalamin-dependent enzymes such as methionine synthase, methylmalonyl-CoA mutase, and diol dehydratase where there are numerous specific
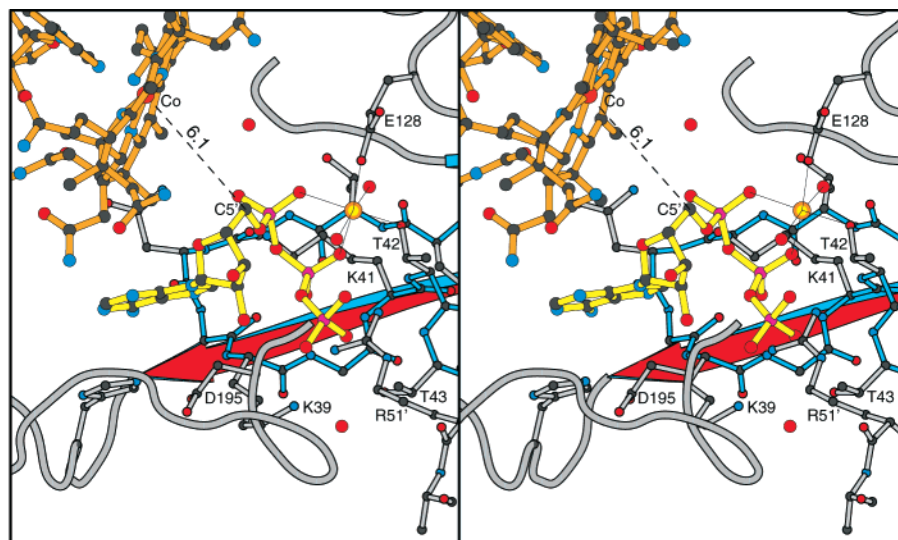
FIGURE 7: Closeup stereoview of the MgATP binding site. All of the side chains that are involved in coordinating the nucleotide are labeled. For clarity, the bonds between the main chain atoms in the P-loop are displayed in cyan. The relationship between C5′ of the ribose and the cobalt of the corrin ring is also visible. This figure was prepared with the programs Molscript and Bobscript (*46*, *47*).

interactions between the side groups of the corrinoid and the protein (*38–40*).

The N-terminal helix is very poorly conserved in CobA homologues and may be missing in thermophiles such as *Pyrococcus horikoshii*. The variability of this component of the structure may play an important role in defining the range of substrates that can be accommodated by a specific enzyme. Likewise, it implies that this helix might be unnecessary for binding some substrates.

It appears that the coordination of the corrin ring is driven by hydrophobic interactions. As shown in Figure 9b, the hydrophobic components of the corrin ring are adjacent to a group of hydrophobic amino acid side chains. This includes Trp[93], Tyr[131], Tyr[135], and Phe[184]. There is also a hydrophobic component to the interaction between the N-terminal α-helix on the adjacent subunit and the nucleotide loop of hydroxycobalamin.

Catalytic and Evolutionary Considerations. Surprisingly, there are no significant hydrogen bonding contacts between the corrinoid and MgATP. This most likely arises because the corrin ring is somewhat distant from MgATP. Indeed, C5′ of the ribose is located ∼6.1 Å from the cobalt which is too far for nucleophilic attack. Although the Co(I) intermediate is highly reactive, it still must be reasonably close to C5′ of the ribose for transfer to occur. This suggests that reduction of the corrinoid to Co(I) is accompanied by a structural rearrangement that brings C5′ of the ribose and cobalt closer together. Although not evident in the electron density, it is anticipated that the coordination sphere of the cobalt in the present structure should be completed by a water molecule since most Co(III) complexes are hexacoordinate. Indeed, there is ample room for a water molecule between C5′ of the ribose and the cobalt ion. Removal of this water molecule from the coordination sphere (if present) must occur prior to reduction to Co(I) because, otherwise, this highly reactive nucleophile might react with water rather than C5′ of the ribose. This suggests that the rearrangement of the ternary complex occurs after reduction of Co(III) to Co(II). Structural studies of the nucleotide hydrolases in the RecA family suggest that the strand between the P-loop and Walker

B motif may be involved in sensing the state of the nucleotide (*41*); however, in CobA, these residues are not in contact with the MgATP. Thus, it is difficult to project how a conformational change is accommodated on the basis of orthologous structures.

As noted previously, the topology of CobA belongs to the P-loop-containing family of nucleotide hydrolases. Within this superfamily, its overall fold is remarkably similar to that of adenosylcobinamide kinase/adenosylcobinamide guanylyltransferase (CobU in *S. typhimurium*), RecA protein, and F₁ATPase (Figure 4). CobU is the enzyme that is responsible for phosphorylating the aminopropanol arm of adenosylcobinamide and, in a subsequent step, activating the cobinamide by the addition of GMP to form adenosylcobinamide-GDP (*42*). This group of proteins shares no measurable level of amino acid sequence similarity, except for the P-loop. Remarkably, the same protein fold, which is fairly unusual within the structural database, is found in two enzymes (CobA and CobU) that are separated by only a few steps in the cobalamin biosynthetic pathway.

Beyond their common folds, the structures of CobA and CobU are quite different. For example, CobA is a dimer, whereas CobU is a trimer. Furthermore, although the corrinoid binding site for CobU is unknown, it seems likely that CobU binds adenosylcobinamide with great specificity in a large groove between protein subunits that lies approximately parallel to the β-sheet in a way that presents the aminopropanol arm of the cobinamide to the γ-phosphate of the ATP. This is in contrast to CobA where the corrin ring lies perpendicular to the β-sheet and presents the center of the corrin ring to C5′ of the ribose held in place by the P-loop. Additionally, CobU is believed to utilize the P-loop in a conventional manner for its kinase reaction. However, CobU is an unusual enzyme since it is a small protein that functions as both a kinase and guanylyltransferase where the transferase activity proceeds through a covalent guanylyl–histidine intermediate (*43*). Interestingly, there is considerable evidence that the kinase and transferase active sites overlap such that in the transferase reaction the GTP binds across the P-loop in the reverse order as seen in CobA (*44*). Thus,
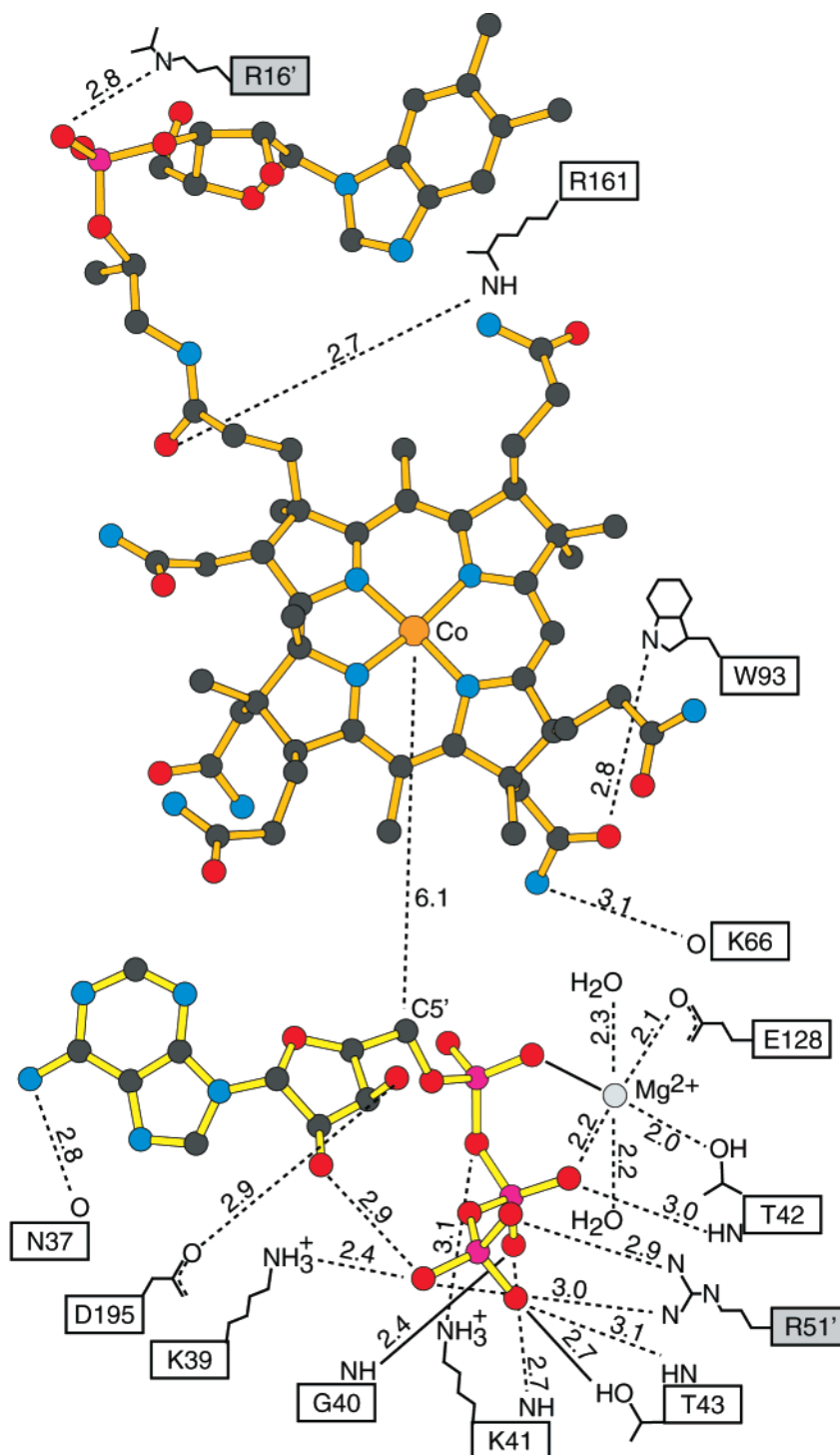
FIGURE 8: Schematic representation of the hydrogen bonding pattern of the protein, MgATP, and hydroxycobalamin. The conformation of the ligands has been distorted from that observed in the ternary complex for clarity. Arg[16′] and Arg[51′] are shaded in gray and indicate side chains from the 2-fold related subunit. This figure was prepared with the programs Molscript and Bobscript (*46*, *47*).

CobA and CobU appear to share the common feature of utilizing their respective P-loops in a novel way to bind their nucleotide substrates.

It has been postulated that CobU arose from a primordial kinase and evolved the ability to function as a transferase because of the disorder−order transition or substrate-induced active site that occurs when the guanylyl nucleotide binds (*44*). The same suggestion can now be applied to CobA. Perhaps it also originated as a kinase that possessed the normal use of the P-loop. The evolutionary significance of the structural similarity between CobA and CobU is un-

known, but provides another intriguing example of the manner in which protein folds have been retooled during evolution.

CONCLUSIONS

The structure described here for the ternary complex of CobA, MgATP, and hydroxycobalamin answers many of the questions that instigated this structural study. It provides an explanation for the kinetic order of substrate binding and the broad specificity of the enzyme. Most likely, this complex
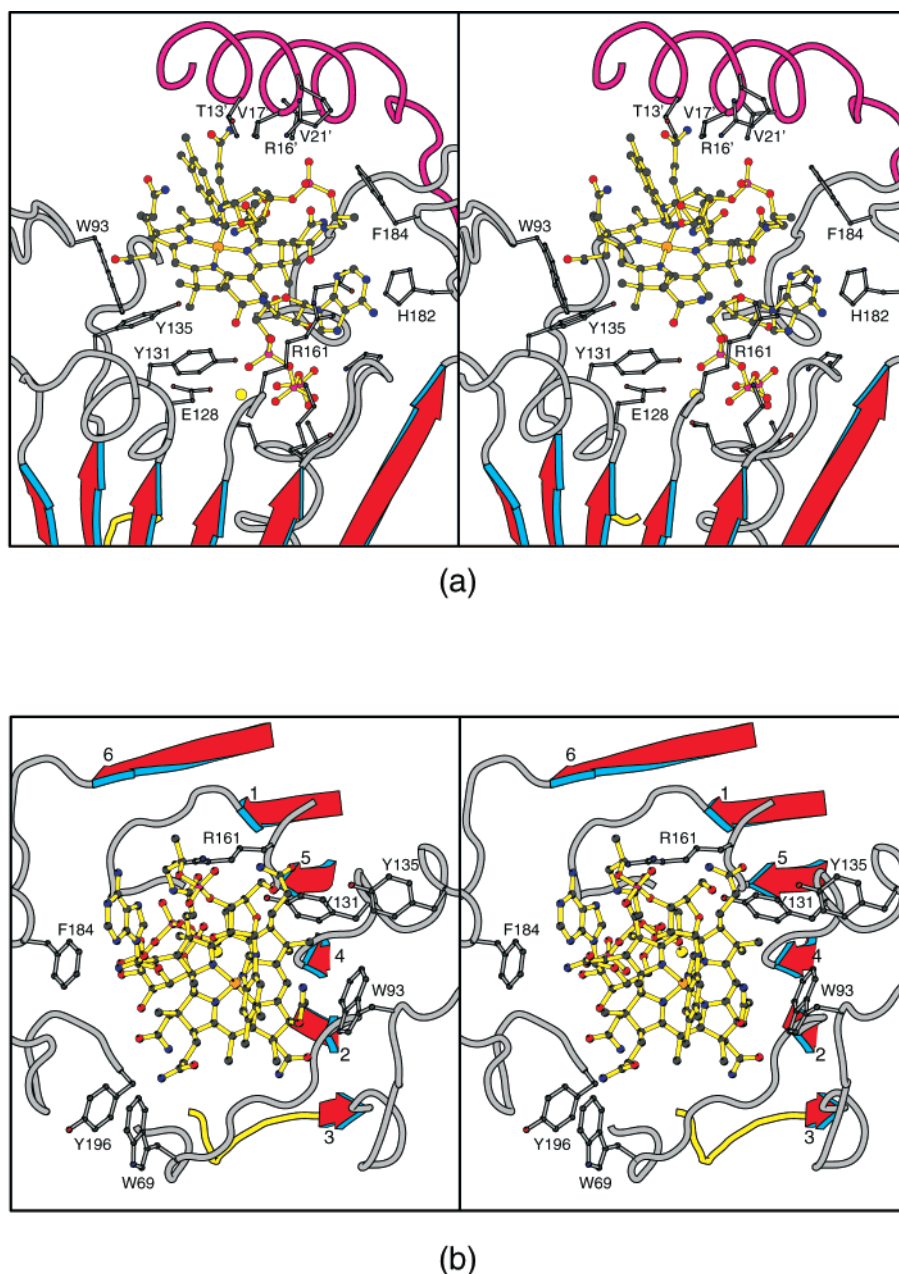
FIGURE 9: Closeup stereoviews of the corrin binding site. A side view to show the capping of the corrin binding pocket by the N-terminal α-helix from the symmetry-related subunit is depicted in panel a. A top view to show the arrangement of hydrophobic ligands in proximity to the hydrophobic components of the corrin ring is shown in panel b. All of the ligands that are involved in coordinating the corrinoid are labeled. This figure was prepared with the programs Molscript and Bobscript (*46*, *47*).

represents the initial structural state in the adenosylation process since it is likely that the reduction to cobalt(I) occurs on the enzyme. The long distance of 6.1 Å between the cobalt of the corrin ring and C5′ of the ribose, however, suggests that a structural rearrangement must occur during reduction of the cobalt(III) to cobalt(I) to facilitate formation of the cobalt−carbon bond. Certainly, water has to be eliminated from the proximity of the cobalt to increase the efficiency of the reaction. The nature of this rearrangement is unknown and awaits further structural and spectroscopic study.

Until recently, little was known regarding the manner in which the cobalt was reduced from Co(III) to Co(I). The reduction occurs in two single-electron transfers. Initially, it was believed that a reductase was necessary for each step, but it has now been reported that endogenous concentrations of dihydroflavins in solution may be sufficient for the reduction from Co(III) to Co(II) (*15*). The second electron transfer cannot be accomplished by dihydroflavins alone and requires a protein to mediate this process. This raises the question of whether there is a specific binding site for a Co-(II) reductase. Given the variety of corrinoids that can be adenosylated by this enzyme and its orthologues in other organisms, it is expected that the protein involved in the electron transfer process will utilize some structural component of the enzyme rather than recognizing the substrate. Examination of the structure reveals the presence of an exposed hydrophobic patch consisting of Trp[69], Pro[70], Met[192], and Tyr[196]. It remains to be proven whether these residues influence the adenosylation reaction. These questions are presently being addressed by additional biochemical and X-ray structural studies.

REFERENCES

1. Blanche, F., Cameron, B., Crouzet, J., Debussche, L., Thibaut, D., Vuilhorgne, M., Leeper, F. J., and Battersby, A. R. (1995) *Angew. Chem., Int. Ed. 34*, 383−411.
2. Rondon, M. R., Trzebiatowski, J. R., and Escalante-Semerena, J. C. (1997) *Prog. Nucleic Acid Res. Mol. Biol. 56*, 347−384.
3. Raux, E., Thermes, C., Heathcote, P., Rambach, A., and Warren, M. J. (1997) *J. Bacteriol. 179*, 3202−3212.
4. Santander, P. J., Roessner, C. A., Stolowich, N. J., Holderman, M. T., and Scott, A. I. (1997) *Chem. Biol. 4*, 659−666.
5. Debussche, L., Couder, M., Thibaut, D., Cameron, B., Crouzet, J., and Blanche, F. (1992) *J. Bacteriol. 174*, 7445−7451.
6. Debussche, L., Couder, M., Thibaut, D., Cameron, B., Crouzet, J., and Blanche, F. (1991) *J. Bacteriol. 173*, 6300−6302.
7. Pezacka, E. H. (1993) *Biochim. Biophys. Acta 1157*, 167−177.
8. Blanche, F., Maton, L., Debussche, L., and Thibaut, D. (1992) *J. Bacteriol. 174*, 7452−7454.
9. Watanabe, F., and Nakano, Y. (1997) *Methods Enzymol. 281*, 289−295.
10. Weissbach, H., Brot, N., and Lovenberg, W. (1966) *J. Biol. Chem. 241*, 317−321.
11. Walker, G. A., Murphy, S., and Huennekens, F. M. (1969) *Arch. Biochem. Biophys. 134*, 95−102.
12. Brady, R. O., Castanera, E. G., and Barker, H. A. (1962) *J. Biol. Chem. 223*, 2325−2332.
13. Hoover, D. M., Jarrett, J. T., Sands, R. H., Dunham, W. R., Ludwig, M. L., and Matthews, R. G. (1997) *Biochemistry 36*, 127−138.
14. Jarrett, J. T., Hoover, D. M., Ludwig, M. L., and Matthews, R. G. (1998) *Biochemistry 37*, 12649−12658.
15. Fonseca, M. V., and Escalante-Semerena, J. C. (2000) *J. Bacteriol. 182*, 4304−4309.
16. Suh, S.-J., and Escalante-Semerena, J. C. (1993) *Gene 129*, 93−97.
17. Suh, S.-J., and Escalante-Semerena, J. C. (1995) *J. Bacteriol. 177*, 921−925.
18. Peterkofsky, A., and Weissbach, H. (1963) *J. Biol. Chem. 238*, 1491−1497.
19. Laemmli, U. K. (1970) *Nature 227*, 680−685.
20. Vogel, H. J., and Bonner, D. M. (1956) *J. Biol. Chem. 218*, 97−106.
21. Otwinowski, Z., and Minor, W. (1997) in *Methods in Enzymology* (Carter, C. W. J., Sweet, R. M., Abelson, J. N., and Simon, M. I., Eds.) pp 307−326, Academic Press, New York.
22. Terwilliger, T. C., and Berendzen, J. (1999) *Acta Crystallogr. D55*, 849−861.
23. Terwilliger, T. C. (1997) in *Methods in Enzymology* (Carter, C. W. J., Sweet, R. M., Abelson, J. N., and Simon, M. I., Eds.) pp 530−537, Academic Press, New York.
24. Brunger, A. T., Adams, P. D., Clore, G. M., DeLano, W. L., Gros, P., Grosse-Kunstleve, R. W., Jiang, J. S., Kuszewski, J., Nilges, M., Pannu, N. S., Read, R. J., Rice, L. M., Simonson, T., and Warren, G. L. (1998) *Acta Crystallogr. D54*, 905−921.
25. Roussel, A., and Cambillau, C. (1991) in *Silicon Graphics Geometry Partners Directory*, Silicon Graphics.
26. Tronrud, D. E. (1997) *Methods Enzymol. 277*, 306−319.
27. Laskowski, R. A., MacArthur, M. W., Moss, D. S., and Thornton, J. M. (1993) *J. Appl. Crystallogr. 26*, 283−291.
28. Collaborative Computational Project No. 4 (1994) *Acta Crystallogr. D50*, 760−763.
29. Cowtan, K., and Main, P. (1998) *Acta Crystallogr. D54*, 487−493.
30. Story, R. M., Weber, I. T., and Steitz, T. A. (1992) *Nature 355*, 318−325.
31. Abrahams, J. P., Leslie, A. G. W., Lutter, R., and Walker, J. E. (1994) *Nature 370*, 621−628.
32. Subramanya, H. S., Bird, L. E., Brannigan, J. A., and Wigley, D. B. (1996) *Nature 384*, 379−383.
33. Thompson, T. B., Thomas, M. G., Escalante-Semerena, J. C., and Rayment, I. (1998) *Biochemistry 37*, 7686−7695.
34. Walker, J. E., Saraste, M., Runswick, M. J., and Gay, N. J. (1982) *EMBO J. 1*, 945−951.
35. Saraste, M., Sibbald, P. R., and Wittinghofer, A. (1990) *Trends Biol. Sci. 15*, 430−434.
36. Smith, C. A., and Rayment, I. (1996) *Biophys. J. 70*, 1590−1602.
37. Cohen, G. H. (1997) *J. Appl. Crystallogr. 30*, 1160−1161.
38. Drennan, C. L., Huang, S., Drummond, J. T., Matthews, R. G., and Ludwig, M. L. (1994) *Science 266*, 1669−1674.
39. Mancia, F., Keep, N. H., Nakagawa, A., Leadlay, P. F., McSweeney, S., Rasmussen, B., Bösecke, P., Diat, O., and Evans, P. R. (1996) *Structure 4*, 339−350.
40. Shibata, N., Masuda, J., Tobimatsu, T., Toraya, T., Suto, K., Morimoto, Y., and Yasuoka, N. (1999) *Struct. Folding Des. 7*, 997−1008.
41. Lenzen, C. U., Steinmann, D., Whiteheart, S. W., and Weis, W. I. (1998) *Cell 94*, 525−536.
42. O'Toole, G. A., and Escalante-Semerena, J. C. (1995) *J. Biol. Chem. 270*, 23560−23569.
43. Thomas, M. G., Thompson, T. B., Rayment, I., and Escalante-Semerena, J. C. (2000) *J. Biol. Chem. 275*, 27576−27586.
44. Thompson, T. B., Thomas, M. G., Escalante-Semerena, J. C., and Rayment, I. (1999) *Biochemistry 38*, 12995−13005.
45. Johnson, M. G., and Escalante-Semerena, J. C. (1992) *J. Biol. Chem. 267*, 13302−13305.
46. Kraulis, P. J. (1991) *J. Appl. Crystallogr. 24*, 946−950.
47. Esnouf, R. M. (1999) *Acta Crystallogr. D55*, 938−940.